TRACKING ORGAN OVERLAP FOR A CONSTRAINED NON-RIGID REGISTRATION ALGORITHM

W. H. Greene[1], S. Chelikani[2], X. Papademetris[1,2], L. H. Staib[1,2], J. P. S Knisely[3] and J. Duncan[1,2]

Departments of [1]Biomedical Engineering, [2]Diagnostic Radiology
and [3]Therapeutic Radiology, Yale University, New Haven, CT, USA

ABSTRACT

This paper tracks organ (prostate, rectum, bladder) overlap in a constrained non-rigid registration (NRR) algorithm to register computed tomographic (CT) images used in external beam prostate radiotherapy. The local motion of the organs is described by a hierarchical multi-resolution FFD based on cubic B-splines. Registration is achieved by minimizing a cost function which is a combination of three functions representing the overlap of the critical organs, image similarity and smoothness of the transformation. The constrained NRR algorithm generated better registration results when compared to an unconstrained NRR algorithm.

Index Terms— Free-Form Deformation, Image Registration, Radiotherapy

1. INTRODUCTION

Prostate cancer is the most commonly diagnosed cancer amongst men in the United States. Approximately 90% of new prostate cancer cases are clinically localized to the prostate and external beam radiotherapy (EBRT) is a viable option[1].

Recent advances in EBRT have led to three-dimensional conformal radiotherapy (3DCRT) and intensity modulated radiotherapy (IMRT). Prostate 3DCRT requires a precise delineation of the target volume and the adjacent critical organs in order to deliver an optimal dose to the prostate with minimal effect on normal tissues. With IMRT, the intensity of each radiation beam is modulated using three-dimensional computed tomographic (3DCT) images to create an intensity pattern that best matches the shape of the tumor, enabling the creation of sharp dose gradients that can maximize the sparing of normal organs at risk. This permits higher radiation doses to be delivered to the tumor with improved tumor control probabilities without increased risk of unwanted normal tissue toxicities, but only if the prostate and adjacent organs' locations are accurately known and accounted for on a daily basis[2]. Because the treatment is delivered in daily fractions over several weeks for both 3DCRT and IMRT, the patient must be precisely and reproducibly positioned in order to ensure that the planned dose is delivered to the prostate.

Development of cone-beam CT (CBCT) imaging systems allow CBCT systems to be anchored to EBRT treatment machines. With both imaging and radiotherapy available on the same platform, daily CBCTs can now be acquired and used for patient positioning. However, a non-rigid registration problem must be solved in order to map the planning day CT image into each treatment day CBCT image.

This paper presents a constrained non-rigid registration algorithm for use in registering the planning day CT image to the treatment day CBCT images. The overlap for the prostate, rectum, and bladder is tracked for each iteration of the NRR algorithm.

2. IMAGE REGISTRATION

The presented registration algorithm minimizes the cost function by maximizing the image intensity similarity, ensuring the transformation is smooth and locally constrained to the predetermined independent transformations of the segmented critical organs.

The algorithm consists of two steps. The first step independently registers each of the segmented critical organs. The second step performs a constrained non-rigid registration, using the control points from the independent organ registrations as constraints.

2.1. Transformation Model

Both steps of the algorithm use a hierarchical multi-resolution FFD transformation model based on cubic B-splines[3]. FFDs deform an object by manipulating the underlying mesh of control points.

A cubic B-spline FFD is defined by designating the image volume as $\Omega = \{(x, y, z)|0 \leq x < X, 0 \leq y < Y, 0 \leq z < Z\}$. Φ denotes a $(l + 3) \times (m + 3) \times (n + 3)$ mesh of control points $\phi_{i,j,k}$ with uniform spacing $\delta_x, \delta_y, \delta_z = \delta$. The parameter domain of the image can be defined as $\Theta = \{(u, v, w)|0 \leq u \leq l, 0 \leq v \leq m, 0 \leq w \leq n\}$. The FFD can then be written as a 3D tensor product of 1D cubic B-splines:

$$T_{0d}(x,y,z) = \sum_{i=0}^{3}\sum_{j=0}^{3}\sum_{k=0}^{3} B_i(u-\lfloor u \rfloor)B_j(v-\lfloor v \rfloor) B_k(w-\lfloor w \rfloor)\phi_{(\lfloor u \rfloor+i)(\lfloor v \rfloor+j)(\lfloor w \rfloor+k)} \quad (1)$$

where T_{0d} is the transformation that maps the planning day image I_0 to the treatment day image I_d and the relationship between the parameter and the image domain is straight forward, $u = \frac{x}{\delta}_x, v = \frac{y}{\delta}_y, w = \frac{z}{\delta_z}$. In addition, B_i represents the i^{th} basis function of the cubic B-spline

$$B_0(u) = \frac{(1-u)^3}{6}$$
$$B_1(u) = \frac{(3u^3 - 6u^2 + 4)}{6}$$
$$B_2(u) = \frac{(-3u^3 + 3u^2 + 3u + 1)}{6}$$
$$B_3(u) = \frac{u^3}{6}.$$

B-splines are locally controlled, which means that moving one control point affects the transformation in the local neighborhood of the manipulated control point[4]. This feature of cubic B-splines makes the control points ideal constraints.

The degree of non-rigid motion captured depends on the resolution of the control points ϕ_{ijk}, which are the parameters of the cubic B-spline FFD. In order to create a computationally efficient algorithm with an adequate degree of non-rigid deformation required to capture the soft tissue motion within the CT images, a hierarchical multi-resolution approach in which the resolution of the control point mesh is increased in a coarse to fine fashion was implemented [3].

2.2. Image Intensity Matching

To determine the relationship between a planning day image and a treatment day image, a similarity criterion which determines the amount of overlap between the two images must be defined. Because we are registering CT to CT in this paper, sum of squared differences, which directly compares image intensities, is used.

$$C_{SSD}(I_d, I_0(T_{0d})) = \sum_{i=0}^{N} \frac{[I_d(i) - I_0(T_{0d}(i))]^2}{N} \quad (2)$$

where i indexes over the voxels. Image overlap is maximized by minimizing C_{SSD}.

2.3. Transformation Smoothing

An injective function is a function which has a unique output for each unique input. Given

$$T : U \rightarrow V$$
$$S : V \rightarrow U$$

then T is injective if $S(T(u)) = u$ for every u in U.

Choi presented sufficient conditions for the local injectivity of a FFD based on cubic B-splines. The injective constraint simply restricts each control point to move within a local sphere of radius $r < R$, where $R \approx 0.4033 \times \delta$ [5, 6]. The injective constraint is used to ensure the transformation is valid

$$C_{smooth}(\Phi) = \sum_{ijk} f(\phi_{ijk}) \quad (3)$$

where

$$f(\phi_{ijk}) = \begin{cases} 0 & \text{if } |\phi_{ijk}| < 0.4033 \\ |\phi_{ijk}| & \text{otherwise} \end{cases}.$$

2.4. Organ Constraints

Each organ ($obj = 1, 2, 3$) is independently registered using binary segmented organs from the planning day I_0 and treatment day I_d images.

Due to the local control of B-Splines, the control points contained within the organ region can be held as constraints in the constrained registration

$$C_{cp}(\Phi) = \sum_{obj}\sum_{ijk} g(\phi_{ijk}^{obj}) \quad (4)$$

where

$$g(\phi_{ijk}^{obj}) = \begin{cases} 0 & \text{if } \phi_{ijk}^{obj} \notin obj \\ 0 & \text{if } |\phi_{ijk}^{obj} - \phi_{ijk}| \leq \gamma \\ |\phi_{ijk}^{obj} - \phi_{ijk}| & \text{otherwise} \end{cases}.$$

Here, γ is the tolerance which is set to 1×10^{-3}.

2.5. Optimization

A different cost function is used for each of the different steps in the algorithm. Both cost functions are minimized using a conjugate gradient method.

2.5.1. Independent Organ Registration

Each organ is independently registered using binary segmented organs from the planning day I_0 and treatment day I_d images. To find the optimal transformation, we minimize a cost function C_{organ} which is a function of C_{SSD} and the injective constraint imposed upon the control points

$$C_{organ}(\Phi) = C_{SSD}\left(T_{0d}(I_0), I_d\right) + \beta C_{smooth}(\Phi). \quad (5)$$

Above, β is the weighting parameter that is set to infinity to ensure the transformation is valid.

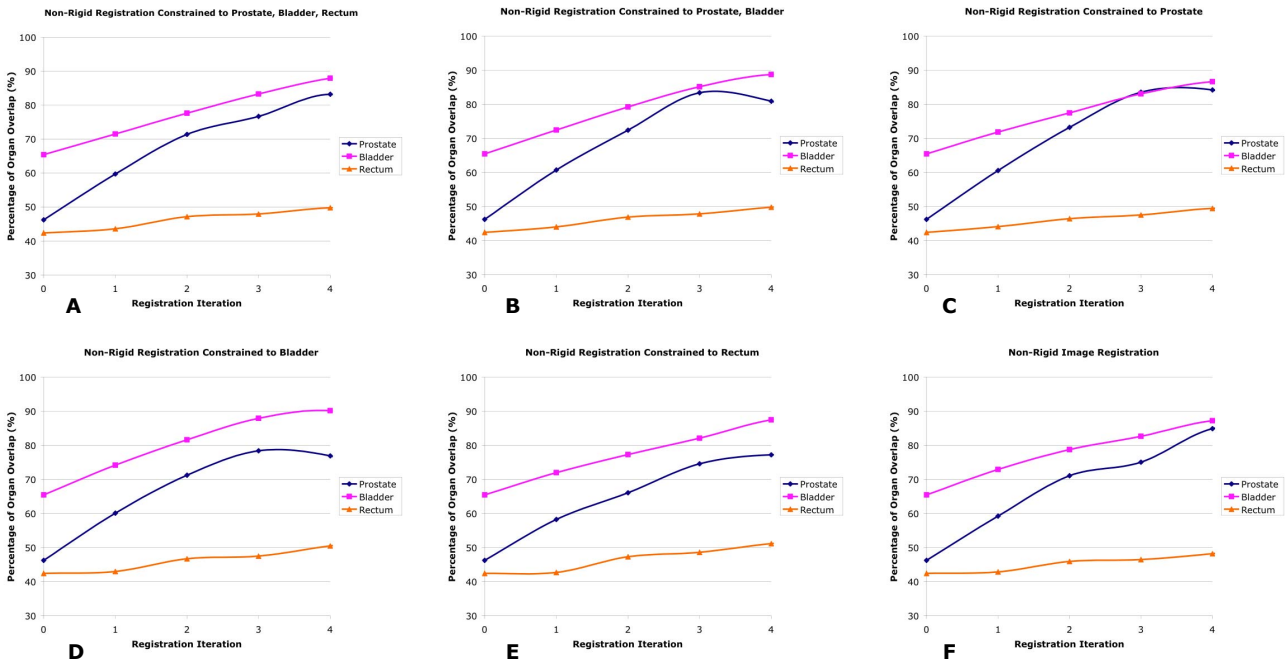

Fig. 1: Constrained NRR results. A: NRR constrained to the prostate, rectum and bladder, B: NRR constrained to the prostate and bladder, C: NRR constrained to the prostate, D: NRR constrained to the bladder, E: NRR constrained to the rectum, F: NRR without constraints.

2.5.2. Constrained Registration

The transformation that maps the planning day image I_0 into the treatment day image I_d is determined by minimizing the constrained registration cost function C. Cost function C is similar to C_{organ} but has the additional term C_{cp} to take into account the control point constraints that are used to align the organs

$$C(\Phi) = C_{SSD}(T_{0d}(I_0), I_d) + \alpha C_{cp}(\Phi) + \beta C_{smooth}(\Phi) \quad (6)$$

where α is the weighting value that determines how loose or tight the organ constraints are held. For the purposes of this paper, α is set to infinity to maximize organ overlap.

3. RESULTS

The algorithm has been tested on real clinical data from a patient undergoing external beam prostate radiotherapy. The original spiral beam CT images had a size of $276 \times 188 \times 137$ voxels and a spatial resolution of $1.17mm \times 1.25mm \times 1.17mm$. To decrease the runtime of the algorithm, the images were resliced to $82 \times 56 \times 41$ voxels with a spatial resolution of $3.94mm \times 4.19mm \times 3.91mm$. The prostate, rectum and bladder were hand segmented by a clinician.

The algorithm was tested with three, two, one and zero organ constraints in order to determine how unconstrained organs are carried along by those that are constrained. Prostate, bladder and rectum overlap were tracked for each iteration of the algorithm.

Registration Level	Control Point Mesh	Control Point Spacing (mm)
1	$11 \times 13 \times 10$	23
2	$19 \times 14 \times 11$	20
3	$21 \times 16 \times 12$	18
4	$23 \times 17 \times 13$	16

Table 1: Control point mesh and spacing at each iteration

The shape and volume of the prostate remain approximately constant from day to day, which greatly aided the quality of registration. In the best registration case, the prostate overlap went from 46.26% to 84.19% when the non-rigid registration was only constrained to the prostate, as seen in Fig. 1(C).

The volume of the bladder varies from day to day, however the shape remains similar and the bladder is an easily segmented structure. Both of these situations led to excellent registration results for the bladder. In the best registration case, the bladder overlap went from 65.44% to 90.11% when only the bladder was held as a constraint in the non-rigid registration, as can be seen in Fig. 1(D).

The rectum is an odd shape which varies from day to day. This variation and irregularity in shape makes the rectum hard to segment and is the reason the rectum had poor registration results when compared to the bladder and prostate results. The initial unaligned rectum overlap was 42.41%. The best

Fig. 2: A: Planning day image I_0, B: Treatment day image I_d, C: Transformed planning day image $I_0(T_{0d})$.

rectum overlap was 51.17%, which was generated when the non-rigid registration was constrained only to the rectum, as seen in Fig. 1(E).

4. CONCLUSION

It was hypothesized that constraining the registration to all three organs would generate the best organ overlap due to the local control of each control point. Local control effectively causes each control point to act as an anchor, pulling along local tissue as it gets deformed. For the case in which ϕ_{ijk} lies in more than one organ, the larger organ was given control of the control point. The results from the registration show that maximal organ overlap for a given organ was achieved when the registration was constrained to that organ. Maximal organ overlap was not achieved when the registration was constrained to three organs due to too many overlapping control point constraints. As the largest organ, the bladder had the best alignment results in every registration in which it was used as a constraint.

To solve the problem of overlapping constraint control points giving full deformation control to the control point that lies within the largest organ, the deformation should be weighted based on the size of the organs that share the control points. For the situation in which ϕ_{ijk} lies in all three organs, the following could be used

$$\phi_{ijk} = \alpha\phi_{ijk}^{blad} + \beta\phi_{ijk}^{rect} + \gamma\phi_{ijk}^{prost}$$

where α, β, γ are the individual organ weights.

Due to the large down sampling of the CT images the image quality was significantly lowered as can be seen in Fig. 2. Due to poor image quality, the finest control point mesh that could be used was $23 \times 17 \times 13$ which generated a control point spacing of $16mm$. Had the images not been down sampled, image quality would have been maintained, more than four iterations could have been used and better results would have been achieved.

Future work will be performed on higher quality images, which will enable more iterations and a finer control point meshs to be used. As well, the method by which overlapping control point constraints are handled will be updated to use a weighted combination of the deformations for the conflicting control point constraints as suggested above.

5. REFERENCES

[1] A. L. Potosky, J. Legler, P. C. Albertsen, J. L. Stanford, F. D. Gilliland, A. S. Hamilton, J. W. Eley, R. A. Stephenson, and L. C. Harlan, "Health outcomes after prostatectomy or radiotherapy for prostate cancer: Results from the prostate cancer outcomes study," J. Nat. Cancer Inst., October 2000, vol. 92, pp. 1582–1592.

[2] S. Chelikani, K. Purushothaman, J Knisely, Z. Chen, R. Nath, R. Bansal, and J. Duncan, "A gradient feature weighted minimax algorithm for registration of multiple portal images to 3DCT volumes in prostate radiotherapy," Int. J. Radiation Oncology Biol. Phys., 2006, vol. 65, pp. 535–547.

[3] D. Rueckert, L. Sonoda, E. Denton, S. Rankin, C. Hayes, M. O. Leach, D. Hill, and D. J. Hawkes, "Comparison and evaluation of rigid and non-rigid registration of breast MR images," SPIE, 1999, vol. 3661, pp. 78–88.

[4] D.F. Rogers, *An Introduction to NURBS: with Historical Perspective*, Morgan Kaufmann Publishers, San Francisco, 1st edition, 2001.

[5] Y. Choi and S. Lee, "Local injectivity conditions of 2D and 3D uniform cubic b-spline functions," 1999, pp. 302–311.

[6] D. Rueckert, P. Aljabar, R.A. Heckemann, J. V. Hajnal, and A. Hammers, "Diffeomorphic registration using b-splines," MICCAI, October 2006.